Am J Physiol Cell Physiol 286: C518–C528, 2004;
10.1152/ajpcell.00280.2003.

Extracellular matrix controls myosin light chain phosphorylation and cell contractility through modulation of cell shape and cytoskeletal prestress

Thomas R. Polte,[1] Gabriel S. Eichler,[1] Ning Wang,[2] and Donald E. Ingber[1]

[1]*Vascular Biology Program, Departments of Pathology and Surgery, Children's Hospital and Harvard Medical School; and*
[2]*Physiology Program, Harvard School of Public Health, Boston, Massachusetts 02115*

Submitted 3 July 2003; accepted in final form 12 October 2003

Polte, Thomas R., Gabriel S. Eichler, Ning Wang, and Donald E. Ingber. Extracellular matrix controls myosin light chain phosphorylation and cell contractility through modulation of cell shape and cytoskeletal prestress. *Am J Physiol Cell Physiol* 286: C518–C528, 2004; 10.1152/ajpcell.00280.2003.—The mechanism by which vascular smooth muscle (VSM) cells modulate their contractility in response to structural cues from extracellular matrix remains poorly understood. When pulmonary VSM cells were cultured on increasing densities of immobilized fibronectin (FN), cell spreading, myosin light chain (MLC) phosphorylation, cytoskeletal prestress (isometric tension in the cell before vasoagonist stimulation), and the active contractile response to the vasoconstrictor endothelin-1 all increased in parallel. In contrast, MLC phosphorylation did not increase when suspended cells were allowed to bind FN-coated microbeads (4.5-μm diameter) or cultured on micrometer-sized (30 × 30 μm) FN islands surrounded by nonadhesive regions that support integrin binding but prevent cell spreading. Cell spreading and MLC phosphorylation also both decreased in parallel when the mechanical compliance of flexible FN substrates was raised. MLC phosphorylation was inhibited independently of cell shape when cytoskeletal prestress was dissipated using a myosin ATPase inhibitor in fully spread cells, whereas it increased to maximal levels when microtubules were disrupted using nocodazole in cells adherent to FN but not in suspended cells. These data demonstrate that changes in cell-extracellular matrix (ECM) interactions modulate smooth muscle cell contractility at the level of biochemical signal transduction and suggest that the mechanism underlying this regulation may involve physical interplay between ECM and the cytoskeleton, such that cell spreading and generation of cytoskeletal tension feed back to promote MLC phosphorylation and further increase tension generation.

fibronectin; cell mechanics; hypertension

VASCULAR SMOOTH MUSCLE (VSM) cell contractility plays a central role in the control of normal vascular physiology and, when deregulated, in the development of bronchopulmonary dysplasia and persistent pulmonary hypertension of the newborn, as well as systemic hypertension. Work on control of VSM cell function has focused on the identification of soluble contractile agonists, such as endothelin-1 (ET-1), that act systemically to stimulate contractility (49). More recent studies, however, have revealed that local signals within the tissue microenvironment may also contribute significantly to contractile control. Most notably, alterations in cell adhesion to extracellular matrix (ECM) or direct interference with integrin receptor binding modulate the contractile response of VSM cells, as well as various nonmuscle cells, both in vitro and in vivo (13, 18, 26, 42). This is important because the abnormal accumulation of ECM that is a hallmark of hypertension is also accompanied by hypercontractility of VSM cells (15, 41, 44, 49). Yet, little is known about how cell interactions with ECM influence this critical behavior.

Cell contractility results from the action of tensional forces that are generated within the actin cytoskeleton. Tension generation results from binding interactions between actin and myosin filaments that activate a myosin ATPase that drives filament sliding. These actin-myosin interactions are promoted by phosphorylation of the regulatory myosin light chain (MLC) (45) by MLC kinase (MLCK) (14). MLCK activity is controlled by intracellular Ca^{2+} and calmodulin levels (45); however, this stimulatory influence is balanced by MLC phosphatase, which can dephosphorylate MLC (16). Various signaling molecules contribute to control of MLC phosphatase activity, including the Rho effector, Rho-associated kinase (ROCK) (16), and protein kinase C (46). Interestingly, binding and clustering of integrin receptors can activate both the Rho (38) and protein kinase C pathways (2, 6, 50, 55).

Cell interactions with ECM differ from those with soluble regulators, because cells also apply traction to their integrin receptors that mediate matrix adhesion (1). Tensional forces generated within the cytoskeleton and resisted by the ECM feed back to alter cell shape and thereby influence various cellular responses, including growth, differentiation, and motility. Importantly, cultured VSM cells exhibit different levels of contractility on ECM substrates that differ in their ability to support cell spreading (26, 47). The Rho/ROCK pathway and associated focal adhesion formation can also be stimulated by increasing the mechanical stiffness of the ECM substrate (13) or by direct distortion of cell surface integrins (1, 31, 39). However, these local events at the site of integrin binding still remain under the control of global biochemical events that are linked to cell distortion: spread VSM cells respond to vasoagonists that work through the Rho pathway (e.g., lysophosphatidic acid), whereas retracted cells do not (47).

Cell shape stability requires the establishment of a mechanical force balance within the cytoskeleton (20). Tensional forces that are generated within contractile microfilaments are partially balanced by the cell's external tethers to the ECM substrate and partly by internal microtubules that resist compression inside the cell. By balancing these forces between microfilaments, microtubules, and ECM, the cell generates a "prestress" or state of isometric tension in the cytoskeleton that mechanically stabilizes cell shape. Moreover, these internal forces can be shifted between these different load-bearing

Address for reprint requests and other correspondence: D. E. Ingber, 11th Floor, New Research Building, Children's Hospital, 300 Longwood Ave., Boston, MA, 02115 (E-mail: donald.ingber@tch.harvard.edu).

The costs of publication of this article were defrayed in part by the payment of page charges. The article must therefore be hereby marked "*advertisement*" in accordance with 18 U.S.C. Section 1734 solely to indicate this fact.

elements. For example, chemical disruption of microtubules increases the level of traction exerted on the ECM as compressive forces normally borne by these cytoskeletal elements are transferred to complementary ECM adhesion sites (51). Conversely, modifying ECM mechanics can also alter the level of forces carried by microtubules and microfilaments (33, 36, 37). The point is that both the level of prestress in the cytoskeleton and the net contractile force cells exert on their ECM substrate depend on a cellular mechanical force balance between the cytoskeleton and the ECM. The purpose of the present study was therefore to gain further insight into the fundamental mechanism by which cell adhesion and spreading on ECM regulate pulmonary VSM cell contractility by exploring whether ECM-dependent changes in this cellular force balance feed back to modulate the contractility set-point.

MATERIALS AND METHODS

Experimental system. VSM cells were isolated from the pulmonary artery of newborn calves (3) and used in the second to fourth passages. Cells were maintained in low glucose DME (JRH Biosciences) supplemented with 2 mM glutamine, 100 U/ml penicillin, 100 U/ml streptomycin, 10 mM HEPES (Life Technologies), and 10% FBS (Hyclone) in 10% CO_2. Confluent monolayers were serum-starved for 72 h in DME containing 0.4% FBS before experiments. Quiescent cell monolayers were dissociated into single cells and plated at low density on various substrates as described previously (26). For experimental manipulation, cells were plated in DME containing 1% BSA, transferrin (5 μg/ml; Collaborative Research), human high-density lipoprotein (10 μg/ml; Intracel), 20 mM HEPES, sodium pyruvate (110 mg/l), penicillin G (100 units/ml), streptomycin (100 μg/ml), and L-glutamine (0.292 mg/ml). In certain experiments, cells were treated with ET-1 (20 nM; Calbiochem), cytochalasin D (1 μg/ml; Sigma), 2,3-butanedione 2-monoxime (BDM) (10 mM; Sigma), or nocodazole (10 μM; Sigma).

Various densities (0–1 $\mu g/cm^2$) of FN (Collaborative Research) were immobilized on nonadhesive, bacteriological, plastic dishes, as described (24). Projected cell areas were determined from phase contrast images using IPLab image analysis software (Scanalytics); at least 20 cells from at least 4 randomly selected fields of each culture dish were analyzed for each condition. For bead-binding experiments, tosyl-activated 4.5 μm beads (Polysciences) were coated with a saturating FN density (50 μg/ml) as described (43). Coated beads were added to suspended cells (20 beads/cell) and rocked at 37°C for 30 min; bead attachment was verified by microscopy. Microfabricated micrometer-sized adhesive islands were produced on glass slides and coated with a saturating density of FN (50 μg/ml) as described (8, 9). Flexible polyacrylamide gel culture substrates were prepared according to published methods (33, 51) and coated with high-density FN (1 $\mu g/cm^2$). The substrate flexibility was manipulated by varying both the total acrylamide concentration (2–4%) and the bis-acrylamide component (0.1–0.5%); the Young's modulus (stiffness) for each substrate was determined as described previously (52).

MLC phosphorylation was assayed using glycerol-PAGE in combination with immunoblotting (12, 51). MLC bands were detected with an anti-MLC monoclonal antibody (MY-21; Sigma). The stoichiometry of MLC phosphorylation (mol PO_4/mol MLC) was determined by densitometry using Scion Image software (Scion). MLC phosphorylation was calculated from the following formula: $(P_1 + 2 \times P_2)/(P_0 + P_1 + P_2)$ where P_0 = unphosphorylated MLC band, P_1 = singly phosphorylated MLC band, and P_2 = doubly phosphorylated MLC band. Microfluorimetric quantitation of intracellular calcium levels was carried out using fura 2 in conjunction with ratio imaging, as described (51).

The tractional stresses exerted by individual cultured VSM cells and cellular prestresses were quantitated using a modified form of traction force microscopy, as previously described (48). Briefly, VSM cells were cultured on flexible polyacrylamide gels substrates (Young's modulus = 3,750 Pa) coated with various densities of fibronectin (0.02 to 1 $\mu g/cm^2$) that contained green fluorescent nanobeads (500-nm diameter; Molecular Probes) as fiducial markers. Nanobead positions were measured before and after addition of warm SDS (1% final concentration) to remove the cells. Isometric tension forces (prestress) exerted by each of the adherent cells were determined by comparing bead position before and after cell detachment and calculating relative bead displacements. Active traction forces produced by stimulation with the vasoagonist, ET-1, were calculated by subtracting the total traction force exerted minus the prestress calculated for cells under similar conditions without ET-1. Statistical analysis of total MLC phosphorylation and prestress was carried out using means calculated from all experiments of a defined condition, and significance was determined by the Student's *t*-test for unpaired samples. The Student's *t*-test for paired samples was used for statistical analysis of changes in MLC phosphorylation and tractional forces induced by various agents.

To confirm changes in the organization of microfilaments and microtubules after drug treatment, cells cultured on glass coverslips (Lab-Tek, Nalge Nunc, Naperville, IL) coated with FN (1 $\mu g/cm^2$) were fixed with 2% paraformaldehye in microtubule stabilization buffer (0.1 M PIPES, pH 6.75, 1 mM EGTA, 1 mM $MgSO_4$, 2 M glycerol, and protease inhibitors) (5, 30). Microtubules were visualized using a mouse monoclonal anti-tubulin primary antibody (Sigma) and a FITC-conjugated anti-mouse IgG secondary antibody (Amersham). Microfilaments were visualized using rhodamine-phalloidin (300 ng/ml; Sigma). Fluorescent images were captured using a Nikon Diaphot 300 inverted microscope and a Photometrics Sensys KAF 1400 charge-coupled device digital camera.

RESULTS

To explore how ECM modulates cell contractility, pulmonary VSM cells were cultured on nonadhesive plastic dishes that were precoated with increasing densities (0–1 $\mu g/cm^2$) of FN. Cell spreading increased as the density of FN was increased (Fig. 1, *A–F*) as previously reported for VSM cells (26), as well as other cell types (21, 29); this was confirmed by quantitating projected cell areas using computerized image analysis (Fig. 1*G*). MLC phosphorylation levels were then measured in cells plated on various FN densities for 5 or 12 h, before and after stimulation with the vasoconstrictor, ET-1, for 2.5 min. MLC phosphorylation was chosen as biochemical readout of contractility based on its central role in modulating cytoskeletal tension generation (45). Steady-state MLC phosphorylation levels, as measured before ET-1 stimulation, increased in direct proportion as FN coating densities were raised and cell spreading was promoted (Fig. 2, *A* and *B*). The magnitude of MLC phosphorylation induced by ET-1 (20 nM ET-1 for 2.5 min) also increased as FN densities were raised (Fig. 2, *A* and *C*). The concentration of ET-1 used in this study has previously been shown to induce optimal contraction in these cells (26), and a time course of MLC phosphorylation after stimulation with ET-1 confirmed that MLC phosphorylation levels peak by 2.5 min after addition (Fig. 2*D*). A similar correlation between projected cell areas and MLC phosphorylation was also observed when cell spreading on high FN (1 $\mu g/cm^2$) was analyzed as a function of time (Fig. 3).

To directly determine whether these FN-dependent changes in MLC phosphorylation resulted in actual changes in cell prestress (level of isometric tension in the cell before vasoagonist addition) and active contraction in the presence of ET-1,

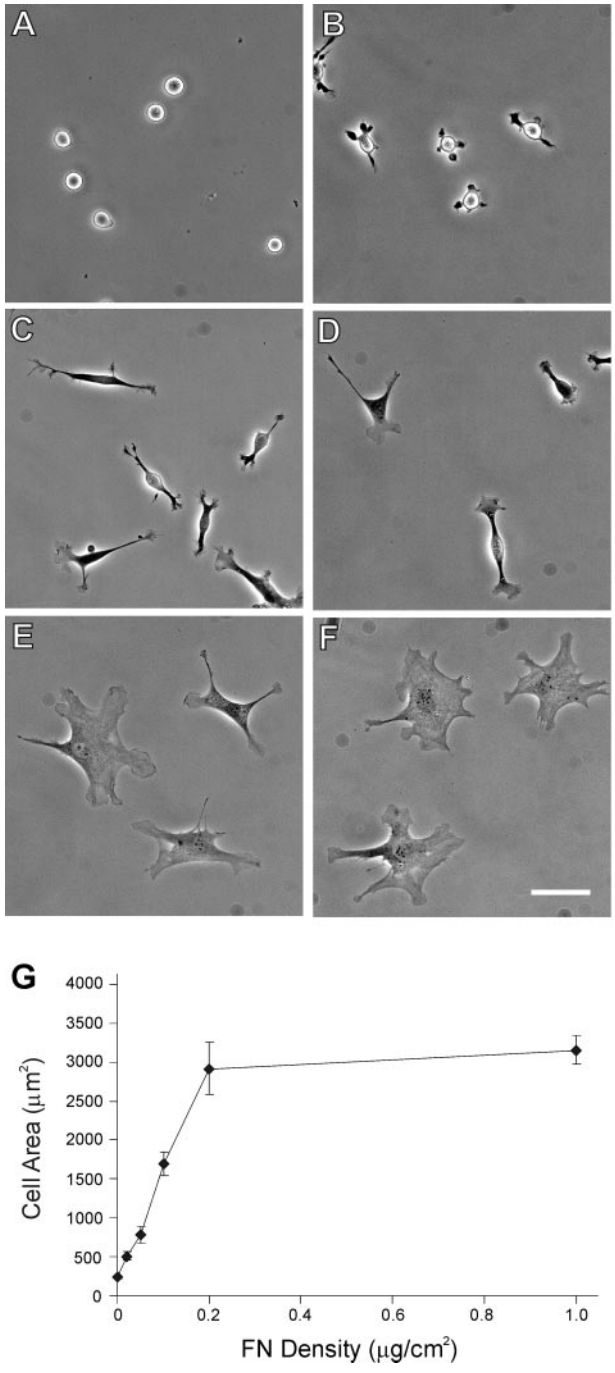

Fig. 1. Control of vascular smooth muscle (VSM) cell shape by varying fibronectin (FN) density. *A–F*: phase contrast views of cells plated for 5 h on dishes coated with 0, 0.02, 0.05, 0.10, 0.20, and 1 μg/cm² FN, respectively. Bar, 50 μm. *G*: projected cell areas as a function of FN coating density (all values are means ± SE).

we measured interfacial traction on the adhesive substrate and cellular prestress within pulmonary VSM cells cultured on flexible, FN-coated, polyacrylamide substrates using traction force microscopy (34, 48). In this technique, cell-generated forces are quantitated by analyzing stress-dependent changes in the movement of small (0.2 μm) fluorescent beads that are contained within the flexible substrate, both before and after removal of the cells from the substrate. Increasing FN coating densities on these flexible substrates resulted in a FN density-dependent increase in cell prestress (Fig. 4*A*). ET-1 induced significant increases in traction at each FN density (Fig. 4*B*). Unlike MLC phosphorylation, the mean net change in traction in response to ET-1 was greatest in cells cultured on moderate FN density (Fig. 4*B*). This result correlated with the fact that a higher percentage of cells demonstrated a statistically significant increase in traction on moderate FN density compared with low and high densities (Fig. 4*C*). However, analysis of ET-1-induced changes in traction in this responsive (contractile) subset of cells again revealed a direct correlation between FN density and the magnitude of ET-1-induced traction forces (Fig. 4*D*). Analysis of the contractile response to ET-1 over time in this same subset of cells (Fig. 4*E*) showed that traction forces closely paralleled MLC phosphorylation (Fig. 2*D*), reaching maximal levels by about 3 min and remaining high through 8 min. Micrographs of responsive cells carried out during traction force microscopy also revealed increases in the number and size of regions where highest traction stresses were exerted beneath individual cells in response to both increasing FN densities and adding ET-1 (Fig. 5).

These initial findings are consistent with the concept that different densities of FN modulate MLC phosphorylation, cell prestress, and the contractile response to ET-1 based on their ability to promote cell extension. However, varying the ECM coating density also alters local integrin receptor clustering and activates associated integrin signaling cascades (24, 28, 43). To discriminate between these two mechanisms, suspended cells were allowed to bind to FN-coated microbeads (4.5-μm diameter), which induce integrin clustering and signaling without promoting VSM cell spreading (28). Cell binding to FN-coated microbeads for 30 min was not sufficient to induce an increase in MLC phosphorylation, either alone or after stimulation with ET-1 (Fig. 6, *A* and *B*).

A potential caveat in these latter experiments is that cells may engulf attached microbeads after periods greater than 30 min (8), thereby limiting the duration of integrin-FN engagement. To address this limitation, cells were cultured for 24 h on microfabricated substrates containing 30 × 30 μm² adhesive islands coated with high FN that limit cell spreading to the size and shape of the islands because they are surrounded by nonadhesive regions (8). Spreading of cells on these small adhesive islands has been shown previously to optimally activate integrin signaling pathways (56). With the use of this method, cell spreading was restricted to ~30% of that observed for cells on control (unpatterned) FN (Fig. 6*C*), and MLC levels were significantly reduced (Fig. 6, *D* and *E*).

The mechanism by which ECM density controls cell extension appears to rest, in part, on the ability of the ECM to physically resist cell tractional forces (23). To independently determine whether the physical properties of the ECM and associated changes in the cellular mechanical force balance are critical for controlling MLC phosphorylation, VSM cells were cultured on flexible substrates that were coated with a constant (saturating) FN density but varied in their mechanical compliance (33). Cells dissipate more stress when adherent to flexible substrates than on rigid dishes that more effectively resist cell-generated tractional forces, and thus the level of prestress in the cytoskeleton is reduced. Cell spreading was suppressed when substrate rigidity (Young's modulus) was decreased (Fig. 7, *A*, *C–F*), as previously observed when FN densities were

lowered (Fig. 1). MLC phosphorylation levels in VSM cells scaled directly with the rigidity of these substrates (Fig. 7*B*) and, hence, with their ability to both maintain isometric tension in the cytoskeleton and support cell spreading.

Because cell spreading decreases as substrate compliance is increased, it could be argued that cell spreading itself is the critical determinant of MLC phosphorylation. To address this possibility, we employed various pharmacological agents that alter cytoskeletal mechanics (and, hence, prestress) in fully spread cells on rigid FN-coated dishes. First, cells were treated with cytochalasin D (1 μg/ml), which disrupts microfilaments (Fig. 8, *A* and *B*) and thus dissipates tensional stress. MLC phosphorylation was greatly reduced in these cells, both before and after stimulation with ET-1 (Fig. 9, *A* and *C*). However, cytochalasin D also has a dramatic effect on cell morphology, inducing cell retraction and rounding (Fig. 8*B*). To dissipate cell prestress without disrupting cytoskeletal integrity or changing cell shape, we used BDM, which inhibits myosin ATPase downstream of MLC phosphorylation (Fig. 8*C*). Computerized image analysis confirmed that BDM did not significantly alter VSM cell spreading under these conditions (average projected cell areas for cells in the presence or absence of BDM were, respectively, 3,241 ± 228 and 3,209 ± 171 μm^2). In spread cells treated with BDM, MLC phosphorylation was significantly reduced (Fig. 9, *A* and *C*) to levels similar to those exhibited by cells on low FN (Fig. 2), on highly flexible substrates (Fig. 7), or by retracted cells treated with cytochalasin D (Fig. 9, *A* and *C*). Although BDM had a potent inhibitory effect in cells on moderate and high FN, it did not produce a significant change in MLC phosphorylation in cells on low FN (Fig. 9*D*). One potential complication of BDM

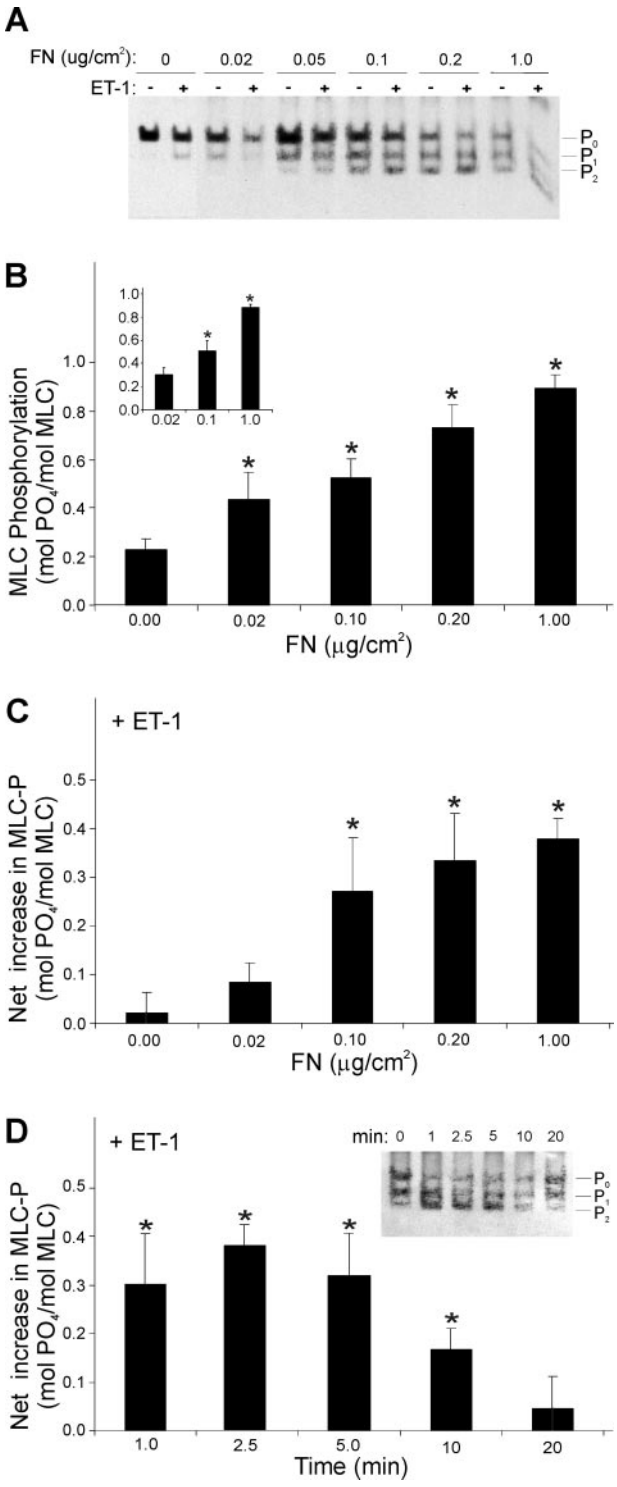

Fig. 2. Control of myosin light chain (MLC) phosphorylation by varying FN density. *A*: immunoblot showing the phosphorylated forms of MLC from cells cultured for 5 h on various densities of FN before (−) or after (+) incubation with endothelin-1 (ET-1) for 2.5 min (P_0, unphosphorylated MLC band; P_1, singly phosphorylated; P_2, doubly phosphorylated). *B*: steady-state levels of MLC phosphorylation at 5 h, as determined from densitometric analysis of the immunoblots. Results are means ± SE from at least 8 experiments. *$P < 0.05$ compared with suspended cells. *Inset*: a similar effect of FN density on MLC phosphorylation after 12 h of plating. *C*: net increase in MLC phosphorylation after stimulation with ET-1 calculated from *A*. Results are means ± SE from 7 experiments. *$P < 0.05$ compared with unstimulated cells at each FN density. *D*: time course of MLC phosphorylation induced by ET-1 in cells on high FN (1 $\mu g/cm^2$). Results are means ± SE from 3 experiments. *$P < 0.05$ compared with unstimulated cells. *Inset* shows a representative immunoblot.

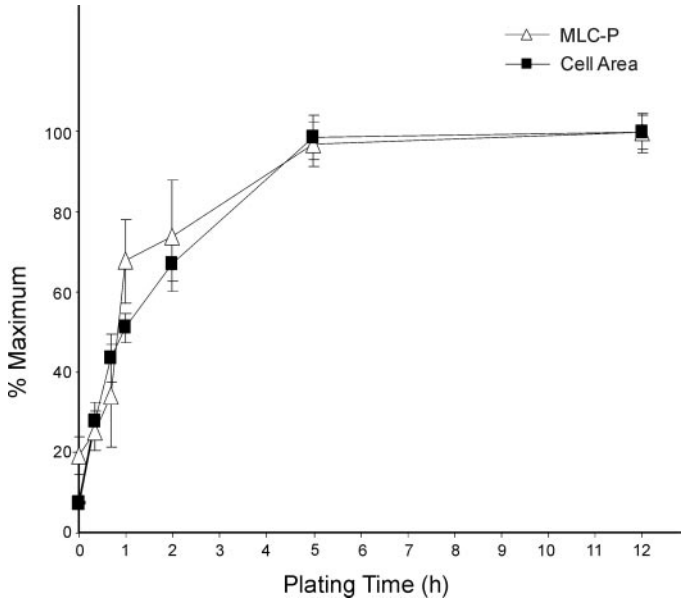

Fig. 3. Comparison of projected cell areas (■) and MLC phosphorylation levels (△) at different times after plating VSM cells on high FN (1 $\mu g/cm^2$). Results are means ± SE from at least 3 experiments normalized to the maximum value obtained within the 12 h time course.

treatment is that it can inhibit calcium transport (4, 32). However, no significant changes in intracellular calcium were detected in BDM-treated VSM cells using the Ca^{2+}-sensitive dye fura 2 and microfluorimetry (data not shown). Treatment of cells with BDM and cytochalasin D also decreased the total level of MLC phosphorylation in ET-1-stimulated cells; however, ET-1 produced a similar net increase in MLC phosphorylation (0.25 to 0.3 mol PO_4/mol MLC) even under conditions in which prestress was dissipated and the cytoskeleton was disrupted (Fig. 9, *A* and *C*).

In contrast to agents that dissipate cellular prestress, treatment of VSM cells with nocodazole at a dose (10 μM) that completely depolymerizes microtubules (Fig. 8, *D* and *E*) elevated MLC phosphorylation to levels comparable to those observed in spread cells maximally stimulated with ET-1 (Fig. 9, *A–C*). Similar induction of MLC phosphorylation by microtubule-disrupting agents has been observed in other cell types (25). Microtubule disruption also was able to increase MLC phosphorylation in cells that were pretreated with either BDM or cytochalasin D to first dissipate cytoskeletal prestress (Fig. 9, *B* and *C*); however, the maximal level of MLC phosphorylation was significantly decreased in the drug-treated cells. This ability of depolymerized microtubules to increase VSM cell contractility required cell adhesion to FN as treatment of suspended cells with the same dose of nocodazole failed to produce any effect on MLC phosphorylation (Fig. 9*E*).

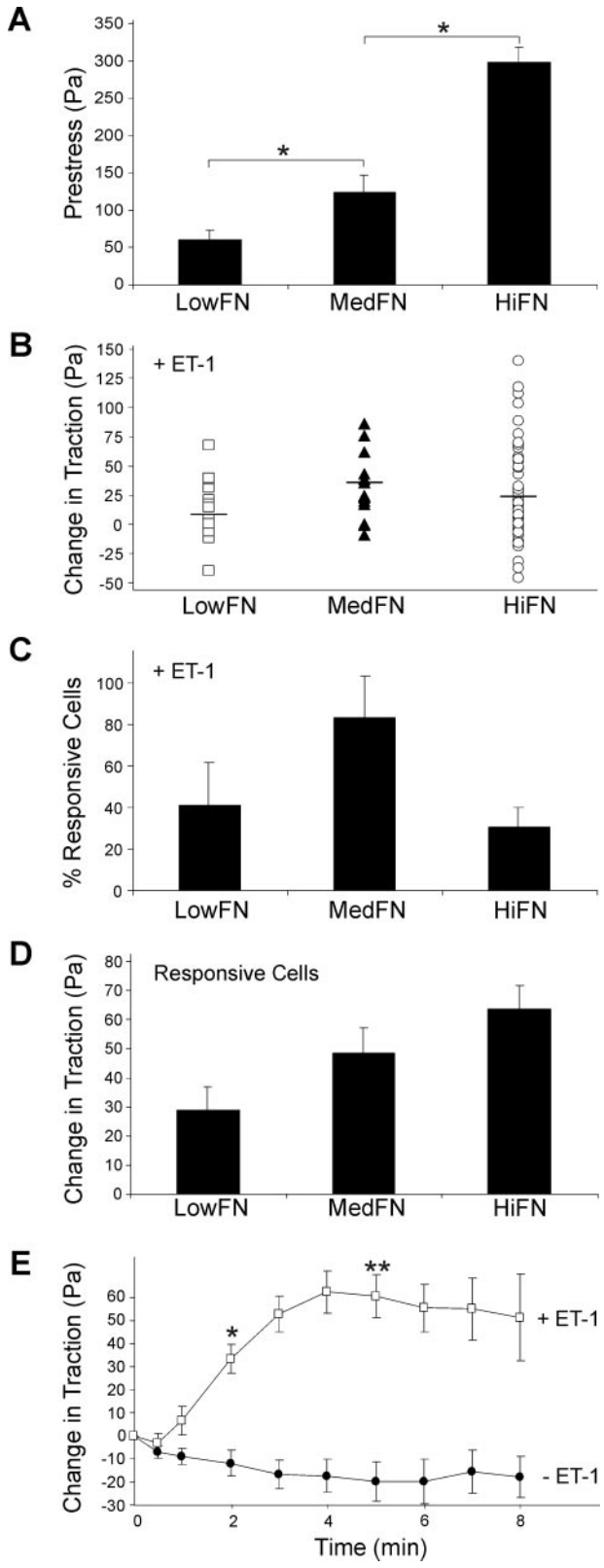

Fig. 4. Quantitation of the effects of FN density on cell prestress and ET-1-induced cell contraction using traction force microscopy. *A*: prestress in cells cultured on low, medium, or high FN densities (0.02, 0.1, or 1 μg/cm^2, respectively) for 12 h. Results are means ± SE from at least 20 cells. *$P <$ 0.05. *B*: scatter-plot representing net change in traction exerted by individual cells cultured on low, medium, or high FN after 5 min treatment with ET-1. Horizontal bar indicates the mean change in traction for each population. The increase in traction was statistically significant ($P < 0.05$) at each FN density. *C*: percentage of responsive cells that demonstrated a significant increase in traction force ($P < 0.05$) compared with untreated cells for each FN density. The percentage of responsive cells at high FN density was significantly less than values from cells on either low or medium FN ($P < 0.05$). *D*: net change in traction after 5 min treatment with ET-1 in the responsive cells shown in *C*. The net change in traction of responsive cells on high FN was significantly greater than values from cells on low FN ($P < 0.05$). Results are means ± SE from at least 10 cells. *E*: time course of net change in traction of cells on high FN after stimulation with ET-1. Results are means ± SE from 14 responsive cells (*$P = 1.12 \times 10^{-5}$; **$P = 6.22 \times 10^{-7}$).

DISCUSSION

In this study, we examined the mechanism by which cell adhesion and spreading on ECM regulate pulmonary VSM cell contractility. In particular, we explored the importance of FN-dependent changes in cell mechanics (i.e., distortion and prestress) for control of contractile signaling, as measured by MLC phosphorylation. Our studies revealed that ECM substrates that promote cell spreading resulted in a concomitant increase in MLC phosphorylation, as well as enhanced responsiveness to the vasoagonist ET-1, whereas suspended cells that completely lacked ECM adhesions failed to significantly increase MLC phosphorylation in response to contractile agonists, including ET-1 and microtubule depolymerization. Similar results were obtained when cell spreading was modulated for 5, 12, or 24 h, indicating that decreasing the FN density or preventing cell spreading did not simply delay the development of normal contractile behavior; rather it altered the set-point for VSM cell prestress and responsiveness to ET-1.

Past studies have shown that biochemical signals are initiated upon integrin engagement and clustering, even in the absence of changes in cell shape or external mechanical load-

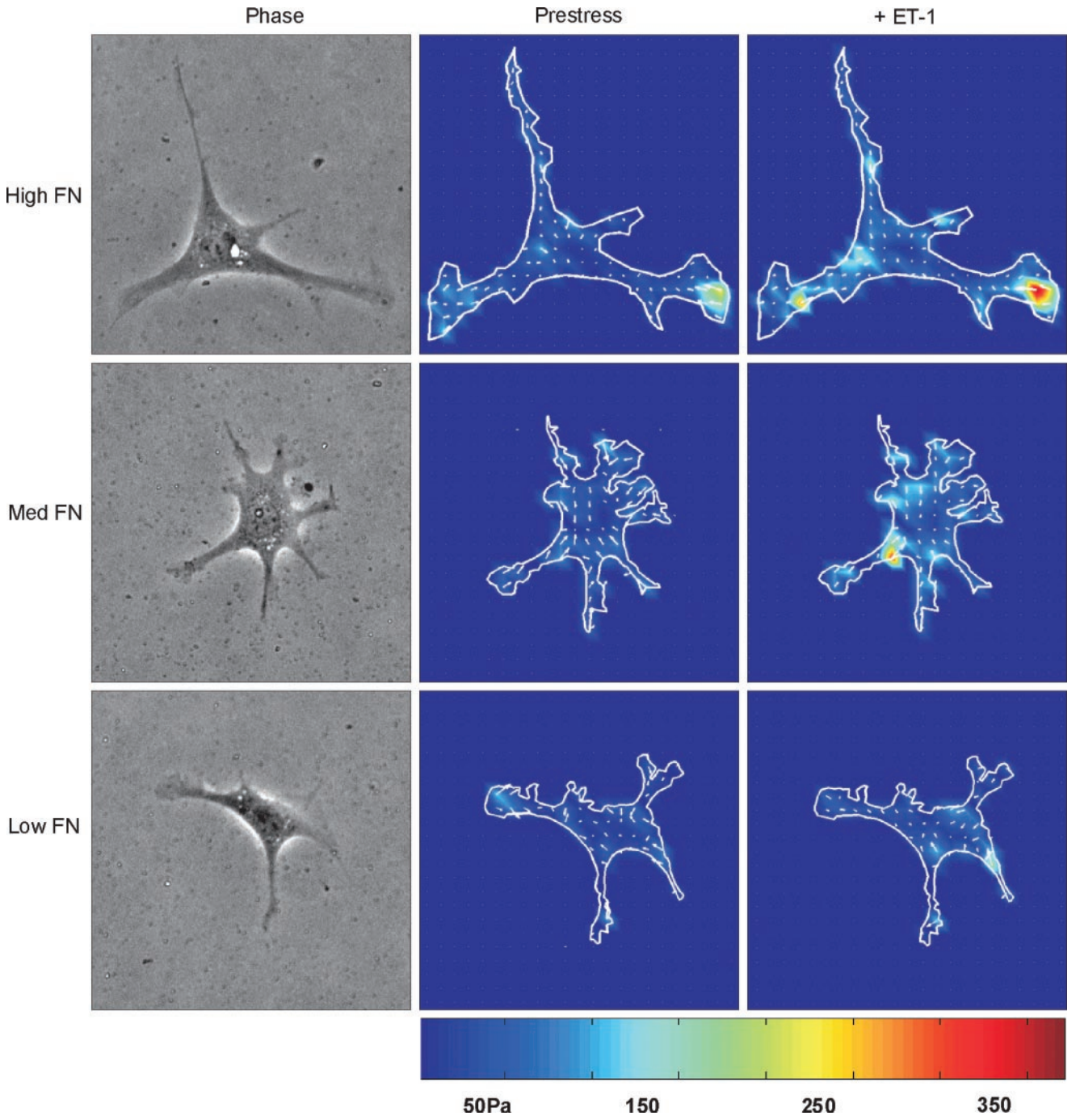

Fig. 5. Quantitation of VSM cell prestress and ET-1-induced contraction using traction force microscopy. Phase contrast views (*left*) and traction field maps of control (*middle*) vs. cells treated with ET-1 (*right*); cells were cultured for 12 h on flexible gels coated with low, medium, or high FN. Small white arrows indicate direction of bead displacements and associated traction stresses. The color scale indicates magnitudes of the tractions in Pascals (Pa); red and orange regions indicate areas of highest concentration of traction stresses.

ing of integrin adhesion sites (28, 35, 43). But in the present study, integrin engagement alone was not sufficient to induce MLC phosphorylation in the absence of cell spreading. Moreover, flexible FN substrates that similarly did not support cell extension also failed to increase MLC phosphorylation. These observations are consistent with the findings of past studies that similarly demonstrated that alterations in the cell that are secondary to integrin binding, specifically, changes in mechanical loading of focal adhesion sites and associated changes in cell shape, are also critical for an integrated contractile response in VSM cells (26, 47). For example, when cells were prevented from spreading using microfabricated elastomeric substrates, they display greatly reduced basal tractional forces (prestress) and failed to contract in response to soluble contractile agonists (serum or lysophosphatidic acid), whereas expression of constitutively active RhoA rescued the contractile response (47).

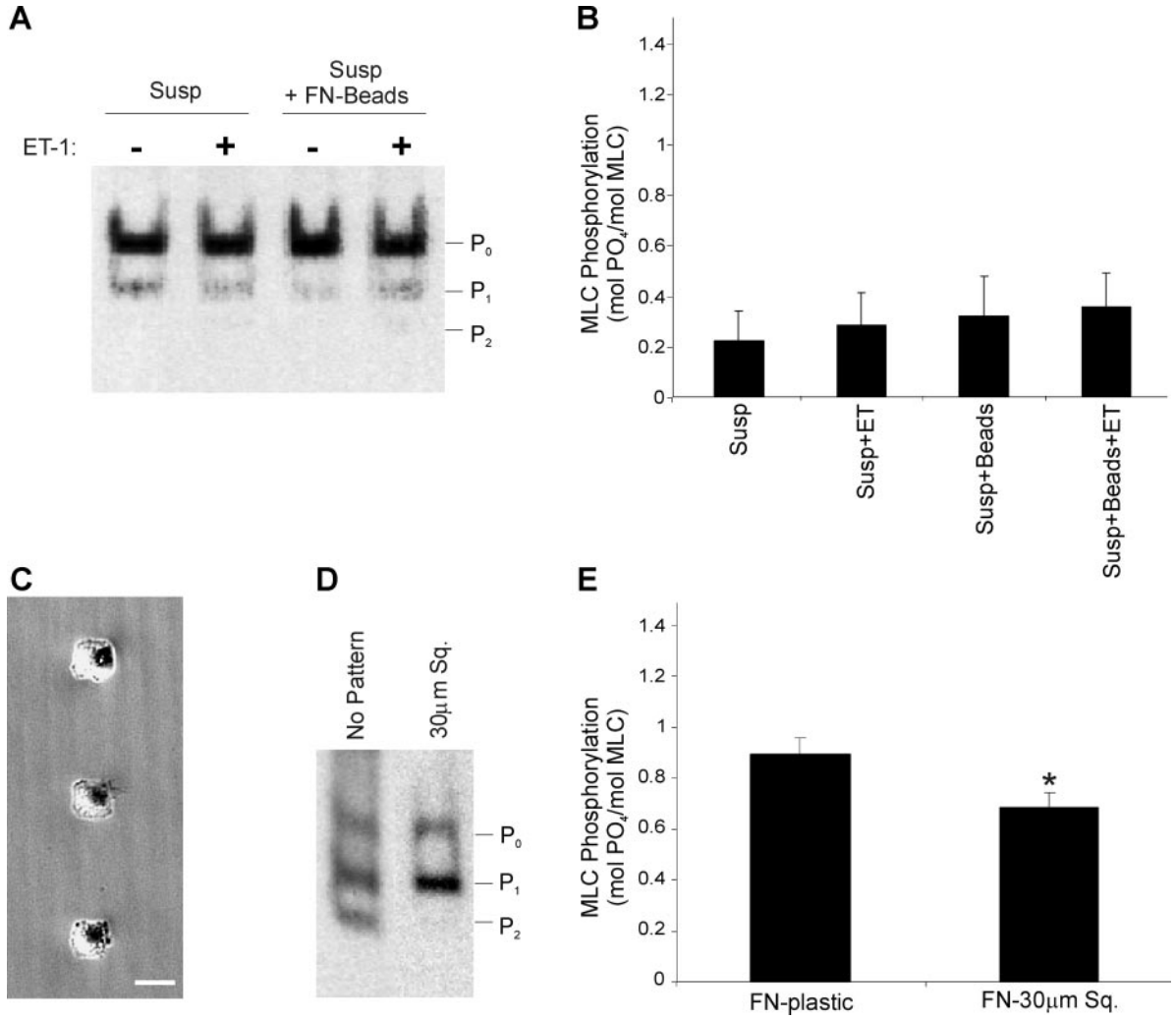

Fig. 6. Effect of integrin binding on MLC phosphorylation in the presence or absence of cell spreading. *A*: immunoblot showing MLC phosphorylation in cells cultured alone in suspension (Susp) or in the presence of FN-beads (Susp + FN-Beads) before (−) and after (+) stimulation with ET-1 for 2.5 min. *B*: stoichiometry of MLC phosphorylation as determined from densitometric analysis of blots shown in *A*. Results are means ± SE from 2 experiments. Differences among values were not statistically significant. *C*: phase contrast image of cells cultured on micropatterned square (30 × 30 μm) adhesive islands (bar, 30 μm). *D*: immunoblot showing MLC phosphorylation in the absence or presence of cell binding to high FN on unpatterned plastic that promotes cells spreading vs. cells on the 30-μm^2 adhesive island that restricts cell extension. *E*: stoichiometry of MLC phosphorylation as determined from densitometric analysis of immunoblot shown in *D*. FN-plastic, cells on high FN for 24 h; 30-μm^2 FN-islands, cells on 30-μm^2 islands coated with high FN for 24 h. Results are means ± SE from at least 3 experiments. *$P < 0.05$ compared with FN-plastic.

The present study extends these findings by showing that ECM-dependent changes in cell spreading modulate signal transduction at the level of MLC phosphorylation, both at steady state and in response to another vasoconstrictor, ET-1. In light of these observations, it is interesting that VSM cells are more responsive to ET-1 on the moderate FN density compared with high FN in terms of increasing the tractional forces they exert on the substrate. A similar relationship between contraction induced by ET-1 and FN density was demonstrated in these same cells using magnetic twisting cytometry (26). This could be explained, in part, if the nonresponsive cells on high FN were already maximally contracted before ET-1 addition. In fact, the mean prestress of the responsive (ET-1-sensitive) cells on high FN was significantly lower than that in the unresponsive cells on the same substrate: 189 ± 29 and 336 ± 21 (Pa, respectively). In contrast, on low FN, both prestress and MLC phosphorylation were low, supporting our argument that contractility is sensitive to cell spreading in these cells.

Nevertheless, it remains unclear how cell spreading impacts biochemical signaling pathways that ultimately modulate MLC phosphorylation and contractility. One potential clue to this mechanism stems from our finding that cell spreading can be dissociated from MLC phosphorylation by altering cell-generated tensile forces independently of cytoskeletal integrity and cell shape. This behavior was observed when actomyosin tension generation was inhibited by BDM, which acts downstream of MLC phosphorylation (17, 27) and does not significantly affect cell shape. Because of BDM's known phosphatase activity (53, 54) and effects on intracellular Ca^{2+} (4, 32),

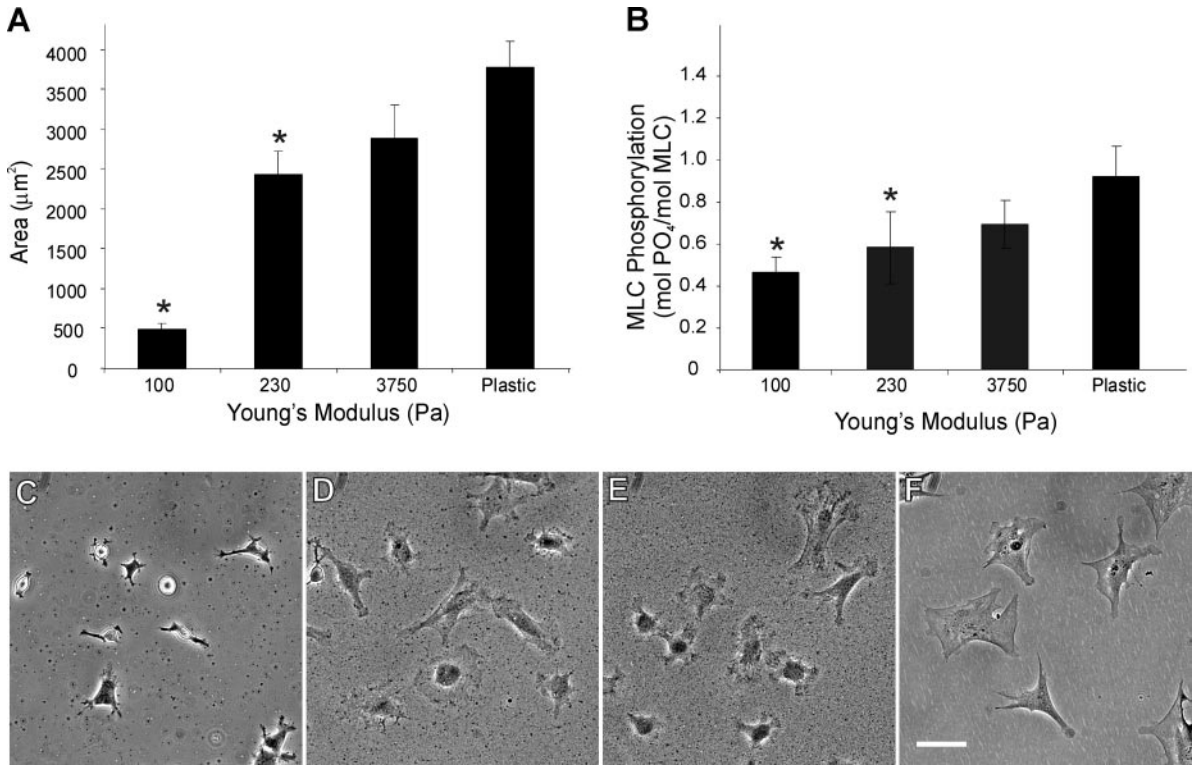

Fig. 7. Modulation of substrate rigidity. *A*: projected cell areas from cells plated for 12 h on substrates of various compliances coated with high FN (1 μg/cm^2). Results are means ± SE from at least 20 cells. *$P < 0.05$ compared with FN-coated plastic. *B*: MLC phosphorylation calculated from cells described in *A.* Results are means ± SE from at least 3 experiments. *$P < 0.05$ compared with FN-coated plastic. *C–F*: phase contrast images of VSM cells plated on FN-coated acrylamide sheets of different stiffness corresponding to Young's moduli of 100 (*C*), 230 (*D*), or 3,750 (*E*) Pa or on FN-coated plastic (*F*) (bar, 50 μm).

we cannot totally exclude the possibility that BDM modulates MLC phosphorylation by pathways separate from its effect on prestress. However, our finding that BDM had only a minimal effect on MLC phosphorylation in cells with low prestress on low FN suggests that its inherent phosphatase activity did not contribute significantly to the results observed under our assay conditions. Likewise, no diminution of intracellular Ca^{2+} was observed in cells treated with BDM in the present study. Thus changes in cytoskeletal prestress that accompany cell spreading may be a key determinant of MLC phosphorylation.

We also found that disruption of microtubules elevated MLC phosphorylation levels in adherent VSM cells, even in cells treated with BDM and cytochalasin D, as previously described (25). These findings indicate that microtubule depolymerization or release of tubule monomers can activate the contractile machinery independently of intact actin filaments or cytoskeletal prestress. However, the total increase in MLC phosphorylation was significantly decreased in cells with lower prestress due to these drug treatments, and the effects of microtubule disruption were completely inhibited in suspended cells that lacked ECM adhesions. Combined with recent findings that demonstrate a direct shift of forces from microtubules to sites of ECM adhesion after microtubule disruption (51), it is possible that part of the observed increases in MLC phosphorylation in adherent cells may be due to changes in tensional forces exerted on ECM adhesions. ET-1 also failed to increase MLC phosphorylation in round cells in suspension, whereas it induced a significant increase in cells adherent to FN that were treated with cytoskeletal disruptor drugs. These findings again suggest that some signaling structure that is formed during the

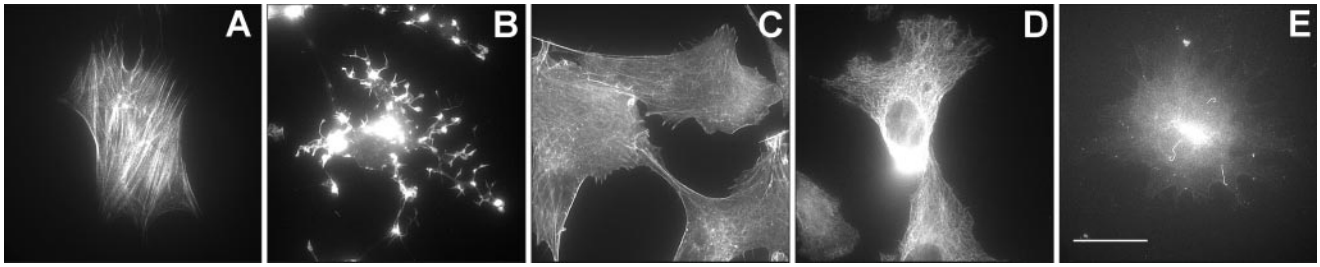

Fig. 8. Effects of cytoskeletal modifiers on cell shape and cytoskeletal organization. Fluorescence micrographs of control cells (*A* and *D*) vs. cells treated for 30 min with 1 μg/ml cytochalasin D (*B*), 30 min with 10 mM 2,3-butanedione 2-monoxime (BDM) (*C*), or 10 min with 10 μM nocodazole (*E*), and stained for microfilaments using rhodamine-phalloidin (*A–C*) or microtubules using anti-tubulin antibodies (*D* and *E*). Bar, 50 μm.

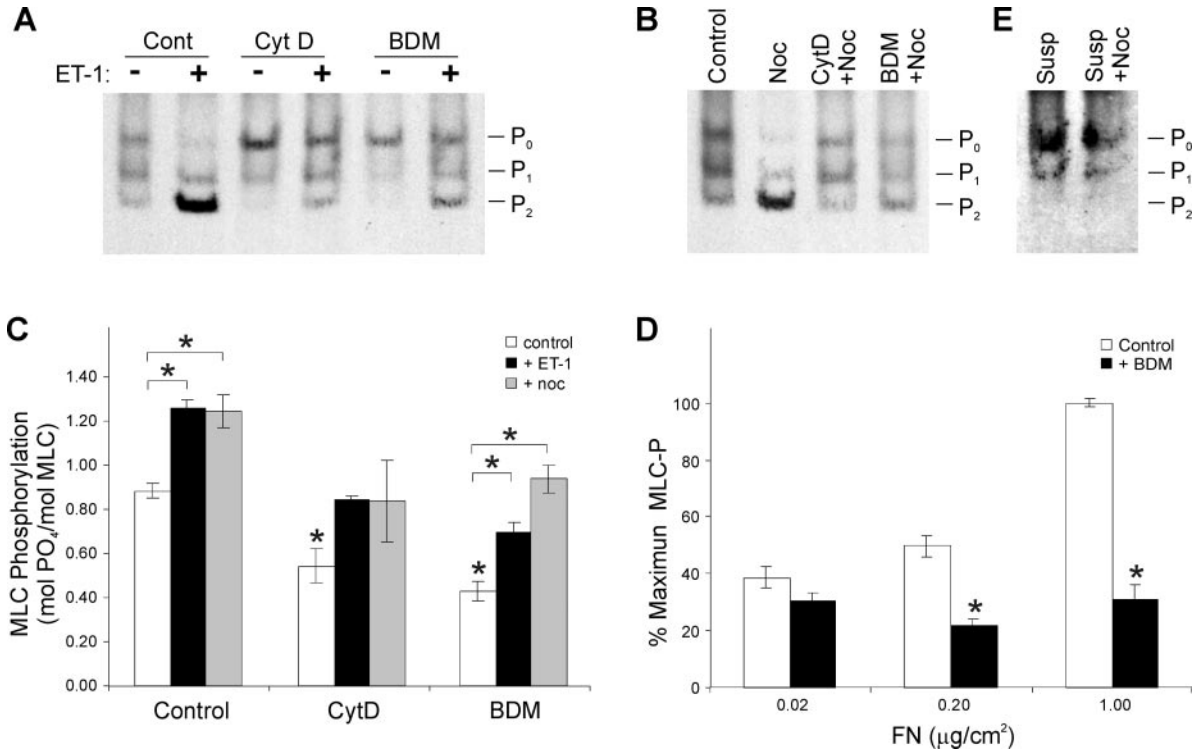

Fig. 9. Effect of modulating cytoskeletal integrity and cytoskeletal prestress on MLC phosphorylation in the presence or absence of ET-1 and nocodazole. *A*: immunoblot showing the various phosphorylated forms of MLC from cells cultured on high FN for 5 h and then treated with either DMSO vehicle (Control), 1 μg/ml cytochalasin D (CytD), or 10 mM BDM (BDM) for 30 min, followed by stimulation with ET-1 for 2.5 min where indicated. *B*: immunoblot showing MLC phosphorylation in cells cultured as in *A* and treated with either DMSO vehicle (Control), 10 μM nocodazole for 10 min (Noc), 1 μg/ml CytD for 20 min, followed by the addition of 10 μm Noc for 10 min (CytD + Noc), or 10 mM BDM for 30 min, followed by the addition of 10 μm Noc for 10 min (BDM + Noc). *C*: stoichiometry of MLC phosphorylation as determined from densitometric analysis of immunoblots shown in *A* and *B*. Results are means ± SE from 3 experiments. *$P < 0.05$ compared with untreated controls. *D*: relative decrease in MLC phosphorylation in cells treated with 10 mM BDM for 30 min after culturing on various densities of FN. Results are presented as the percentage of maximum MLC phosphorylation exhibited by untreated cells on high FN. Values are means ± SE from 2 experiments. *$P < 0.05$ compared with untreated cells at each FN density. *E*: immunoblot showing MLC phosphorylation from VSM cells held in suspension for 30 min before (Susp) or after treatment with 10 μM nocodazole for 10 min (Susp + Noc).

initial process of cell spreading, and is sufficient to support vasoagonist signaling in the absence of prestress, may remain intact under these disruptive conditions. Interestingly, the focal adhesion exhibits this property at least for the short times (minutes) examined in this study.

How might cell spreading and prestress influence biochemical signaling leading to MLC phosphorylation? Increases in cell spreading, cytoskeletal prestress, and microtubule disassembly are all accompanied by increases in traction forces exerted on the ECM (52), which, in turn, promote focal adhesion formation (7, 11, 39). Thus changes in cell shape and prestress may modulate focal adhesion signaling pathways that control MLC phosphorylation. A likely candidate for mediating this type of signaling is RhoA acting through ROCK. Alternatively, prestress may alter the conformation and/or kinetics of other biochemical regulators that are tethered to the cytoskeleton (22).

Whatever the mechanism, the results of this study raise the intriguing possibility that prestress may feed back to regulate contractile signaling, much as it regulates growth signaling (19, 40) and ET-1 gene expression (10). Specifically, our findings suggest that if tension is dissipated in the cytoskeleton (i.e., prestress is decreased) because adhesion sites are of insufficient strength or the compliance of ECM increases, then the cell will remain in a low state of contractility, regardless of the presence of soluble vasoagonists. This contractile set-point is reflected by the level of MLC phosphorylation in the cell before stimulation by soluble agonists, and it is governed by the level of prestress in the cytoskeleton independently of integrin binding or cell spreading. In this way, ECM mechanics may feed back via a mechanochemical mechanism to modulate further tension generation so that an appropriate cellular force balance is achieved to match the physical characteristics of the microenvironment, thereby ensuring "compliance matching" within the vascular wall. These data also suggest that chemical agents that alter ECM mechanics, cytoskeletal structure, or basal prestress may be useful for treatment of hypertensive diseases that are characterized by abnormal VSM cell contractility.

GRANTS

This work was supported by National Heart, Lung, and Blood Institute Grant HL-67669 (to D. E. Ingber) and National Aeronautics and Space Administration Grant NAG2-1509 (to N. Wang).

REFERENCES

1. **Aikawa R, Komuro I, Yamazaki T, Zou Y, Kudoh S, Zhu W, Kadowaki T, and Yazaki Y.** Rho family small G proteins play critical roles in mechanical stress-induced hypertrophic responses in cardiac myocytes. *Circ Res* 84: 458–466, 1999.
2. **Auer KL and Jacobson BS.** Beta 1 integrins signal lipid second messengers required during cell adhesion. *Mol Biol Cell* 6: 1305–1313, 1995.
3. **Benitz WE, Lessler DS, Coulson JD, and Bernfield M.** Heparin inhibits proliferation of fetal vascular smooth muscle cells in the absence of platelet-derived growth factor. *J Cell Physiol* 127: 1–7, 1986.
4. **Blanchard EM, Smith GL, Allen DG, and Alpert NR.** The effects of 2,3-butanedione monoxime on initial heat, tension and aequorin light output of ferret papillary muscles. *Pflügers Arch* 416: 219–221, 1990.
5. **Caron J, Jones AL, and Kirschner MW.** Autoregulation of tubulin synthesis in hepatocytes and fibroblasts. *J Cell Biol* 101: 1763–1772, 1985.
6. **Chang ZL, Beezhold DH, Personius CD, and Shen ZL.** Fibronectin cell-binding domain triggered transmembrane signal transduction in human monocytes. *J Leukoc Biol* 53: 79–85, 1993.
7. **Chen CS, Alonso JL, Ostuni E, Whitesides GM, and Ingber DE.** Cell shape provides global control of focal adhesion assembly. *Biochem Biophys Res Commun* 307: 355–361, 2003.
8. **Chen CS, Mrksich M, Huang S, Whitesides GM, and Ingber DE.** Geometric control of cell life and death. *Science* 276: 1425–1428, 1997.
9. **Chen CS, Ostuni E, Whitesides GM, and Ingber DE.** Using self-assembled monolayers to pattern ECM proteins and cells on substrates. *Methods Mol Biol* 139: 209–219, 2000.
10. **Chen J, Fabry B, Schiffrin EL, and Wang N.** Twisting integrin receptors increases endothelin-1 gene expression in endothelial cells. *Am J Physiol Cell Physiol* 280: C1475–C1484, 2001.
11. **Chrzanowska WM and Burridge K.** Rho-stimulated contractility drives the formation of stress fibers and focal adhesions. *J Cell Biol* 133: 1403–1415, 1996.
12. **Daniel JL and Sellers JR.** Purification and characterization of platelet myosin. *Methods Enzymol* 215: 78–88, 1992.
13. **Galbraith CG and Sheetz MP.** Forces on adhesive contacts affect cell function. *Curr Opin Cell Biol* 10: 566–571, 1998.
14. **Gallagher PJ, Herring BP, and Stull JT.** Myosin light chain kinases. *J Muscle Res Cell Motil* 18: 1–16, 1997.
15. **Hadrava V, Tremblay J, and Hamet P.** Abnormalities in growth characteristics of aortic smooth muscle cells in spontaneously hypertensive rats. *Hypertension* 13: 589–597, 1989.
16. **Hartshorne DJ, Ito M, and Erdodi F.** Myosin light chain phosphatase: subunit composition, interactions and regulation. *J Muscle Res Cell Motil* 19: 325–341, 1998.
17. **Herrmann C, Wray J, Travers F, and Barman T.** Effect of 2,3-butanedione monoxime on mysoin and myofibrillar ATPases. An example of an uncompetitive inhibitor. *Biochemistry* 31: 12227–12232, 1992.
18. **Hocking DC, Sottile J, and Langenbach KJ.** Stimulation of integrin-mediated cell contractility by fibronectin polymerization. *J Biol Chem* 275: 10673–10682, 2000.
19. **Huang S, Chen CS, and Ingber DE.** Control of cyclin D1, p27(Kip1), and cell cycle progression in human capillary endothelial cells by cell shape and cytoskeletal tension. *Mol Biol Cell* 9: 3179–3193, 1998.
20. **Ingber DE.** Cellular tensegrity revisited. I. Cell structure and hierarchical systems biology. *J Cell Sci* 116: 1157–1173, 2003.
21. **Ingber DE.** Fibronectin controls capillary endothelial cell growth by modulating cell shape. *Proc Natl Acad Sci USA* 87: 3579–3583, 1990.
22. **Ingber DE.** Tensegrity: the architectural basis of cellular mechanotransduction. *Annu Rev Physiol* 59: 575–599, 1997.
23. **Ingber DE and Folkman J.** Mechanochemical switching between growth and differentiation during fibroblast growth factor-stimulated angiogenesis in vitro: role of extracellular matrix. *J Cell Biol* 109: 317–330, 1989.
24. **Ingber DE, Prusty D, Frangioni JV, Cragoe EJ Jr, Lechene C, and Schwartz MA.** Control of intracellular pH and growth by fibronectin in capillary endothelial cells. *J Cell Biol* 110: 1803–1811, 1990.
25. **Kolodney MS and Elson EL.** Contraction due to microtubule disruption is associated with increased phosphorylation of myosin regulatory light chain. *Proc Natl Acad Sci USA* 92: 10252–10256, 1995.
26. **Lee KM, Tsai KY, Wang N, and Ingber DE.** Extracellular matrix and pulmonary hypertension: control of vascular smooth muscle cell contractility. *Am J Physiol Heart Circ Physiol* 274: H76–H82, 1998.
27. **McKillop DF, Fortune NS, Ranatunga KW, and Geeves MA.** The influence of 2,3-butanedione 2-monoxime (BDM) on the interaction between actin and mysoin in solution and in skinned muscle fibres. *J Muscle Res Cell Motil* 15: 309–318, 1994.
28. **McNamee HP, Liley HG, and Ingber DE.** Integrin-dependent control of inositol lipid synthesis in vascular endothelial cells and smooth muscle cells. *Exp Cell Res* 224: 116–122, 1996.
29. **Mooney D, Hansen L, Vacanti J, Langer R, Farmer S, and Ingber D.** Switching from differentiation to growth in hepatocytes: control by extracellular matrix. *J Cell Physiol* 151: 497–505, 1992.
30. **Mooney DJ, Hansen LK, Langer R, Vacanti JP, and Ingber DE.** Extracellular matrix controls tubulin monomer levels in hepatocytes by regulating protein turnover. *Mol Biol Cell* 5: 1281–1288, 1994.
31. **Numaguchi K, Eguchi S, Yamakawa T, Motley ED, and Inagami T.** Mechanotransduction of rat aortic vascular smooth muscle cells requires RhoA and intact actin filaments. *Circ Res* 85: 5–11, 1999.
32. **Osterman A, Arner A, and Malmqvist U.** Effects of 2,3-butanedione monoxime on activation of contraction and crossbridge kinetics in intact and chemically skinned smooth muscle fibres from guinea pig *taenia coli*. *J Muscle Res Cell Motil* 14: 186–194, 1993.
33. **Pelham, RJ Jr and Wang Y.** Cell locomotion and focal adhesions are regulated by substrate flexibility. *Proc Natl Acad Sci USA* 94: 13661–13665, 1997.
34. **Pelham, RJ Jr and Wang Y.** High resolution detection of mechanical forces exerted by locomoting fibroblasts on the substrate. *Mol Biol Cell* 10: 935–945, 1999.
35. **Plopper GE, McNamee HP, Dike LE, Bojanowski K, and Ingber DE.** Convergence of integrin and growth factor receptor signaling pathways within the focal adhesion complex. *Mol Biol Cell* 6: 1349–1365, 1995.
36. **Putnam AJ, Cunningham JJ, Dennis RG, Linderman JJ, and Mooney DJ.** Microtubule assembly is regulated by externally applied strain in cultured smooth muscle cells. *J Cell Sci* 111: 3379–3387, 1998.
37. **Putnam AJ, Schultz K, and Mooney DJ.** Control of microtubule assembly by extracellular matrix and externally applied strain. *Am J Physiol Cell Physiol* 280: C556–C564, 2001.
38. **Ren XD, Kiosses WB, and Schwartz MA.** Regulation of the small GTP-binding protein Rho by cell adhesion and the cytoskeleton. *EMBO J* 18: 578–585, 1999.
39. **Riveline D, Zamir E, Balaban NQ, Schwarz US, Ishizaki T, Narumiya S, Kam Z, Geiger B, and Bershadsky AD.** Focal contacts as mechanosensors: externally applied local mechanical force induces growth of focal contacts by an mDia1-dependent and ROCK-independent mechanism. *J Cell Biol* 153: 1175–1186, 2001.
40. **Roovers K and Assoian RK.** Effects of rho kinase and actin stress fibers on sustained extracellular signal-regulated kinase activity and activation of g_1 phase cyclin-dependent kinases. *Mol Cell Biol* 23: 4283–4294, 2003.
41. **Saltis J, Agrotis A, and Bobik A.** Differences in growth characteristics of vascular smooth muscle from spontaneously hypertensive and Wistar-Kyoto rats are growth factor dependent. *J Hypertens* 11: 629–637, 1993.
42. **Schnapp LM, Goswami S, Rienzi N, Koteliansky VE, Gotwals P, and Schachter EN.** Integrins inhibit angiotensin II-induced contraction in rat aortic rings. *Regul Pept* 77: 177–183, 1998.
43. **Schwartz MA, Lechene C, and Ingber DE.** Insoluble fibronectin activates the Na/H antiporter by clustering and immobilizing integrin alpha 5 beta 1, independent of cell shape. *Proc Natl Acad Sci USA* 88: 7849–7853, 1991.
44. **Scott-Burden T, Resink TJ, Hahn AW, and Buhler FR.** Angiotensin-induced growth related metabolism is activated in cultured smooth muscle cells from spontaneously hypertensive rats and Wistar-Kyoto rats. *Am J Hypertens* 4: 183–188, 1991.

45. **Somlyo AP and Somlyo AV.** Signal transduction and regulation in smooth muscle. *Nature* 372: 231–236, 1994. [Corrigenda. *Nature* 372: Dec 22–29, 1994, p. 812].
46. **Takuwa Y.** Regulation of vascular smooth muscle contraction. The roles of Ca^{2+}, protein kinase C and myosin light chain phosphatase. *Jpn Heart J* 37: 793–813, 1996.
47. **Tan JL, Tien J, Pirone DM, Gray DS, Bhadriraju K, and Chen CS.** Cells lying on a bed of microneedles: an approach to isolate mechanical force. *Proc Natl Acad Sci USA* 100: 1484–1489, 2003.
48. **Tolic-Norrelykke IM, Butler JP, Chen J, and Wang N.** Spatial and temporal traction response in human airway smooth muscle cells. *Am J Physiol Cell Physiol* 283: C1254–C1266, 2002.
49. **Veyssier-Belot C and Cacoub P.** Role of endothelial and smooth muscle cells in the physiopathology and treatment management of pulmonary hypertension. *Cardiovasc Res* 44: 274–282, 1999.
50. **Vuori K and Ruoslahti E.** Activation of protein kinase C precedes alpha 5 beta 1 integrin- mediated cell spreading on fibronectin. *J Biol Chem* 268: 21459–21462, 1993.
51. **Wang N, Naruse K, Stamenovic D, Fredberg JJ, Mijailovich SM, Tolic-Norrelykke IM, Polte T, Mannix R, and Ingber DE.** Mechanical behavior in living cells consistent with the tensegrity model. *Proc Natl Acad Sci USA* 98: 7765–7770, 2001.
52. **Wang N, Tolic-Norrelykke IM, Chen J, Mijailovich SM, Butler JP, Fredberg JJ, and Stamenovic D. Cell prestress. I.** Stiffness and prestress are closely associated in adherent contractile cells. *Am J Physiol Cell Physiol* 282: C606–C616, 2002.
53. **Waurick R, Knapp J, Ban Aken H, Boknik P, Neunamm J, and Schmitz W.** Effect of 2,3-butandione monoxime on force of contraction and protein phosphorylation in bovine smooth muscle. *Naunyn Schmiedebergs Arch Pharmacol* 359: 484–492, 1999.
54. **Wilson IT and Ginsburg S.** A powerful reactivator of alkyl-phosphate inhibited actylchlinesterase. *Biochem Biophys Res Commun* 18: 168–170, 1955.
55. **Xu J and Clark RA.** A three-dimensional collagen lattice induces protein kinase C-zeta activity: role in alpha2 integrin and collagenase mRNA expression. *J Cell Biol* 136: 473–483, 1997.
56. **Yan L, Moses MA, Huang S, and Ingber DE.** Adhesion-dependent control of matrix metalloproteinase-2 activation in human capillary endothelial cells. *J Cell Sci* 113: 3979–3987, 2000.